Nuclear Instruments and Methods in Physics Research A 1069 (2024) 169845

Contents lists available at ScienceDirect

Nuclear Inst. and Methods in Physics Research, A

journal homepage: www.elsevier.com/locate/nima

Full Length Article

Active dosimetry for VHEE FLASH radiotherapy using beam profile monitors and charge measurements

Vilde F. Rieker [a,b,*], Roberto Corsini [a], Steinar Stapnes [a], Erik Adli [b], Wilfrid Farabolini [a], Veljko Grilj [e], Kyrre N. Sjobak [b], Laurence M. Wroe [a], Avni Aksoy [a,d], Cameron S. Robertson [c], Joseph J. Bateman [c], Pierre Korysko [a,c], Alexander Malyzhenkov [a], Antonio Gilardi [a], Manjit Dosanjh [c]

[a] *European Organization for Nuclear Research, Genève 23, 1211, Switzerland*
[b] *University of Oslo, Postboks 1048 Blindern, Oslo, 0316, Norway*
[c] *University of Oxford, Parks Road, Oxford, OX1 3PU, United Kingdom*
[d] *University of Ankara, Dögol Caddesi, Tandoğan, Ankara, 06100, Turkey*
[e] *Centre Hospitalier Universitaire Vaudois, Rue du Bugnon 46, Lausanne, 1011, Switzerland*

ARTICLE INFO

Keywords:
Dosimetry
UHDR
VHEE
Radiochromic films
Beam profile monitor
YAG

ABSTRACT

The discovery of the FLASH effect has revealed a high potential for treating cancer more efficiently by sparing healthy tissue. The surge in related medical research activities over the last couple of years has triggered a demand for technology with the capability of generating and measuring ionizing radiation at ultra-high dose-rates (UHDR). A reliable dosimetry system is an integral part of a radiotherapy machine. Because existing active dosimetry methods are unable to handle the dose-rates required for FLASH, UHDR dosimetry has emerged as an important area of research. In this paper we present an active dosimetry method based on a scintillating screen and an integrating current transformer. This method provides a simultaneous measurement of the absolute dose delivery as well as the 2D dose distribution. The measurements have been correlated with corresponding readings from radiochromic films (RCFs), and a procedure for image processing has been established. Moreover, different methods of calibrating the active dosimetry system against RCFs have been introduced and evaluated. Lastly, we present results which demonstrate that an agreement with RCFs of better than 5% can be realistically expected if camera parameters are carefully optimized.

1. Introduction

FLASH radiotherapy has become an important field of cancer research because of its potential for highly beneficial therapeutic effects. The optimum therapeutic effect is often described as maximizing the tumour control, while minimizing damage to healthy tissue. By delivering the prescribed dose at ultra-high dose-rates (UHDR), sparing of healthy tissue compared with conventional treatment at low dose-rates has been observed. Moreover, UHDR seems to have the same treatment effect on cancerous tissue as conventional dose rates [1]. The combination of these two observations, termed the FLASH effect, makes radiotherapy at UHDR a promising future modality for treating cancer.

Several research groups of biologists, radiation oncologists and medical physicists around the world are working on understanding the underlying biological mechanisms that govern the FLASH effect. Along with the rapid advances in the field, there is an increasing demand to develop technology capable of delivering the required particle beams. For clinical research in radiation oncology, accelerators and instrumentation for dose delivery control and quality assurance, that can operate reliably and reproducibly under the required conditions, need to be developed. For FLASH beam conditions physicists are therefore studying how to obtain the required beam parameters for UHDR with high precision and reproducibility. Moreover, accurate and reliable dosimetry is crucial. The response of conventional active dosimeters such as ion chambers is nonlinear and tends to saturate at UHDR. More specifically, ion chambers exhibit a significant reduction in collection efficiency at high dose-per-pulse [2,3]. Alternative approaches to active dose monitoring at UHDR have therefore become an important field of research.

In contrast, most passive dosimeters, such as radiochromic films (RCF), exhibit a dose-rate independent nature [4–7]. However, due to their lack of temporal information as well as their manual and

---

* Corresponding author at: European Organization for Nuclear Research, Genève 23, 1211, Switzerland.
E-mail address: vilde.rieker@cern.ch (V.F. Rieker).

https://doi.org/10.1016/j.nima.2024.169845
Received 28 June 2024; Received in revised form 2 September 2024; Accepted 4 September 2024

time consuming procedures for data acquisition, they are not suitable for clinical use. A large scientific community has therefore become invested in optimizing existing methods, as well as developing new tools for active dosimetry at UHDR. One such approach is to exploit the beam instrumentation already present in the accelerator to establish a calibrated "beam-based" dosimetry method. By using measurements of the transverse profile and charge of the particle beam, it would be possible to deduce the resulting dose distribution in a given target.

The CERN Linear Electron Accelerator for Research (CLEAR), is a versatile research linac that can be used for dose distribution measurements for UHDR. The linac is designed for optimal performance at ∼200 MeV. With the ability to easily tune the charge per particle bunch, the number of particle bunches per pulse and the pulse frequency at CLEAR, we can effectively tune the dose-rate over a large range. Combined with the high nominal energy, this dose-rate flexibility makes it one of few machines available for studying FLASH radiotherapy with very high energy electrons (VHEE). Being less sensitive to tissue inhomogeneities than protons, VHEEs can be particularly beneficial for treating large and deep seated tumours [8].

At CLEAR, we are collaborating with biologists and radiation oncologists who are studying the potential benefits of VHEE combined with UHDR. An important part of this collaboration is developing dosimetry methods adapted for VHEE FLASH radiotherapy. Our approach consists of monitoring the charge using an integrating current transformer (ICT) which is inherently non-destructive. We then combine the charge measurement with the transverse beam profile to obtain the transverse charge distribution. The beam profile is monitored via a thin and minimally disruptive yttrium aluminium garnet (YAG) scintillating screen. These screens exhibit sufficient light-yield for a range of beam charges—and a decay time which is suitable for the frequency of the image acquisition system and temporal structure of the beam at CLEAR.

Finally, the key element in verifying a beam-based dosimetry system is to calibrate it with a referenced dosimeter, such as radiochromic films (RCFs). In addition to dose-rate independence, RCFs have the benefit of providing spatial information about the dose distribution. RCFs are thus in themselves (passive) instruments for beam profile measurements, and their dose distributions can be directly correlated with the charge distributions obtained from the beam instrumentation. This paper presents the developments at CLEAR in establishing a procedure for active, beam-based UHDR dosimetry using RCFs as passive reference.

2. Experimental setup

2.1. Beamline description

The travelling-wave accelerating structures (ACS) at CLEAR have a frequency of 3 GHz, and the klystrons that power them have an adjustable pulse repetition rate between 0.833 and 10 Hz. A photo injector generates electron bunches, which can be injected in every single or every other radio frequency (RF) bucket. This flexibility provides the option of 1.5 or 3 GHz bunch frequency. It is also possible to adjust the number of bunches sent with every RF pulse from 1 to ∼150. Lastly, the power of the drive laser can be adapted to tune the bunch charge up to around 1500 pC. The graph in Fig. 1 illustrates these properties.

Together, these properties make CLEAR a well suited linac for exploring the requirement for the FLASH effect by varying beam structures and dose-rates.

Fig. 2 shows a simplified overview of the beamline [9]. Along the beamline, there are several in-vacuum positions equipped with screen plus camera systems (beam television, or BTV) and quadrupoles (QFD and QDD). Respectively, these instruments allow for observation, and tuning of the transverse beam distribution. There are two spectrometer lines with dipoles for quantification of the beam energy [10]. Moreover, both in-air test stands are equipped with BTVs and ICTs, which provide real-time information about the final beam profile and charge per pulse. The robotic sample handling system used for dosimetry studies is installed in air, at the final test stand.

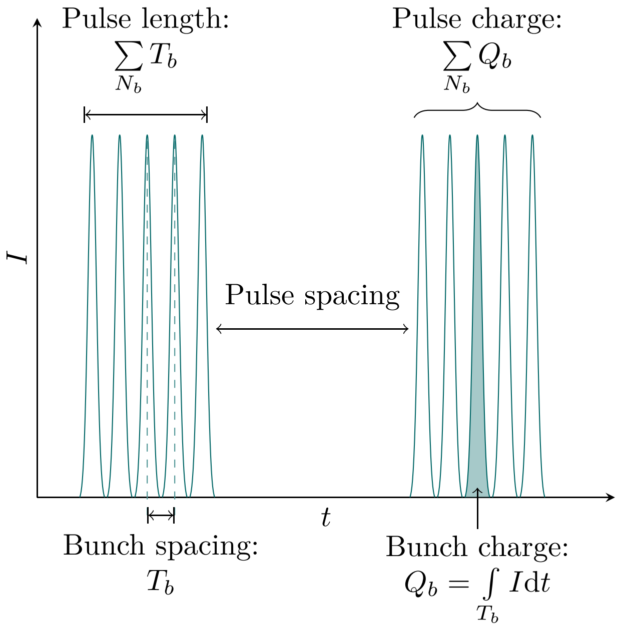

Fig. 1. An illustration of the beam structure at CLEAR.

For the purpose of these studies, we define two separate beam delivery conditions: FLASH and CONV. At CLEAR, FLASH conditions are obtained by sending a single pulse composed of multiple bunches, while CONV, which refers to conventional dose rate, is obtained by delivering multiple single-bunch pulses. Because we are also interested in evaluating the dose-rate dependency of a dosimetric system, we target the same dose in both FLASH and CONV. Effectively, targeting the same dose means targeting the same total charge, under the assumption that tuning the beam's temporal structure does not affect the transverse beam distribution.

There are a number of ways to obtain the same total charge between FLASH and CONV. For CONV, the relevant parameters are the bunch charge, pulse repetition rate and number of pulses delivered. In FLASH there is the bunch charge, the bunch frequency, and the number of bunches in the pulse. The optimal dose-rate for the biological FLASH effect is not yet fully established. Thus, from a dosimetry perspective, the main goal is to develop a system which exhibits a linear response in the full operating range from conventional dose-rates to UHDR.

In these experiments, we aimed to keep the bunch charge constant between FLASH and CONV. Moreover, the instantaneous dose-rate can still be relatively high even with a single bunch pulse. To ensure that the CONV dose-rate was as low as possible, we chose a relatively low bunch charge. Finally, we wanted to target 10 Gy in water as this is a clinically relevant dose. These considerations resulted in the beam parameters summarized in Table 1.

2.2. Sample handling

Our goal is to develop a reliable real time dosimeter for FLASH radiotherapy. Because human tissue mostly consists of water, a water phantom is commonly used for reference dosimetry. However, in a clinical setting, one would typically measure the delivered dose before the patient, correlating it to the one delivered to the patient's organs. It is therefore fundamental to establish the relationship between measurements of beam profiles and dose in both air and water.

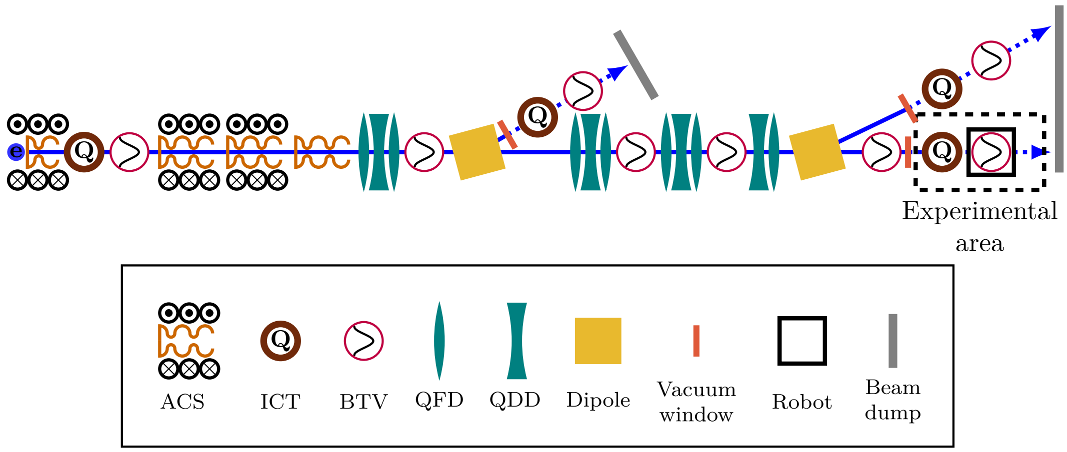

Fig. 2. A simplified drawing of the CLEAR beamline. The YAG screens and the RCFs are positioned within the robot inside the experimental area.

Table 1
Approximate beam parameters used during the experiments, defining the CONV and FLASH conditions. For FLASH, all the charge is delivered within a single pulse beam pulse.

Beam parameters				
Variable	Sym.	Unit	CONV	FLASH
Bunch charge	Q_b	pC	~100	~100
No. of bunches	N_b	1	1	~100
Bunch freq.	f_b	GHz	NA	1.5
No. of pulses	N_P	1	~100	1
Pulse rep. rate	f_P	Hz	0.833	NA
Mean dose rate	$\dot{D}$	Gy/s	**~0.025**	**~10^9**
Delivery time	Δt	s	**120**	**$67 \cdot 10^{-9}$**

Table 2
Details of the beam profile monitoring systems.

Beam charge and profile monitor	
Camera	Basler acA1920-40gm [12]
YAG1	Crytur YAG:Ce, $40 \times 40 \times 0.5$ mm^3 [13]
YAG2	Crytur YAG:Ce, $30 \times 30 \times 0.2$ mm^3 [13]
Pixel size	34 μm
Charge	Bergoz ICT-082-070-5.0 + BCM-IHR-E [14]

Table 3
Details of the RCFs and scanner.

Radiochromic film dosimeters	
Film type	Gafchromic$^{\text{TM}}$ HD-V2 10–1000 Gy [15]
Film dimensions	40×35 mm^2
Scanner	Epson$^{®}$ Perfection V800
Scanning resolution	300 dpi
Pixel size	85 μm

In order to study the relationship between the two media, while ensuring efficient and reproducible data collection, a robotic system has been used. Such a robot was developed in CLEAR in order to move samples in and out of the beam without accessing the accelerator hall, thus enabling the collection of large data sets in a short time [11]. Fig. 3(a) shows a drawing of the robotic system holding a YAG screen in front of the beam. One of the robot's main features is a grabber arm with a camera attached to it, that can pick up custom 3D printed holders. The robotic system allows us to customize holders for both profile monitors and radiochromic films, and thus ensure that they are irradiated under comparable conditions. The robot is installed at the end of the beamline in air. In combination with a water phantom mounted on a vertical stage within the range of the robot grabber, one can easily compare in-air and in-water measurements. The robot can position samples in a relatively large area, and also has the ability to perform longitudinal scans with a profile monitor in the beam direction, which allows us to study the beam evolution through water or air.

2.3. Charge and profile monitoring system

In these studies, we acquired the beam profile by using cerium activated yttrium aluminium garnet (YAG:Ce) scintillating crystals. YAG screens of two different thicknesses, herein referred to as YAG1 and YAG2, were used. The screens were oriented perpendicular to the beam, and the scintillation light was reflected towards a vertically displaced digital camera by a mirror located downstream of the YAG. Moreover, in order to maximize the light intensity reaching the camera, both screens had a thin aluminium coating on the upstream face. The coated YAG screen and mirror was mounted in a 3D printed holder adapted for the robot, which can be seen in Fig. 3(b). The camera was mounted on the robot arm, and the physical pixel size of the full profile monitor was calibrated via physical marks on the YAG screen. The details of the monitoring system are outlined in Table 2.

2.4. Radiochromic films

RCFs come in different compositions with dynamic ranges adapted for different dose ranges. For radiotherapy applications, the doses typically ranges from one Gray up to a few tens of Gray. The ultimate goal of this study is to extend the calibration of the beam-based dosimetry system from air to water, such that one may predict the dose in water from measurements in air. It is therefore meaningful to test the system in air, with a total charge which corresponds to a clinically meaningful dose (e.g. ~10 Gy) in water. For a beam in air at CLEAR, the 1σ–beam size will typically be in the order of 1–2 mm, depending on the exact beam parameters and distance from the vacuum window. In contrast, the same beam in water can easily achieve sizes of 5–6 mm due to the increased scattering. Thus, for the same charge required to achieve a dose of about 10 Gy in water, a dose of in the order of ~100 Gy will be measured in air. The Gafchromic$^{\text{TM}}$ HD-V2 RCF which has a dynamic dose range from 10 to 1000 Gy was therefore selected. The films were cut to rectangles using a laser cutter. The properties of RCFs can be seen in Table 3.

The holders for the RCFs were designed to allow for several films placed longitudinally ~5 mm apart in the same holder, as seen in Fig. 3(c). This design makes it possible to evaluate the longitudinal evolution of the dose distribution in air.

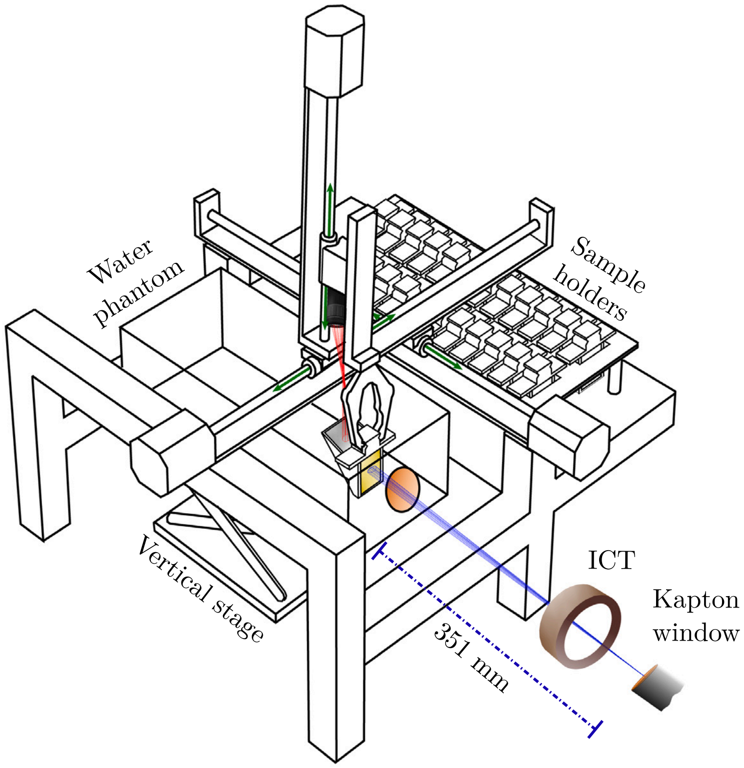

(a) The robot holding the YAG screen perpendicular to the beam. The path of the beam is indicated in blue, while the red lines illustrate the scintillation light which is reflected towards the camera via the mirror behind the YAG.

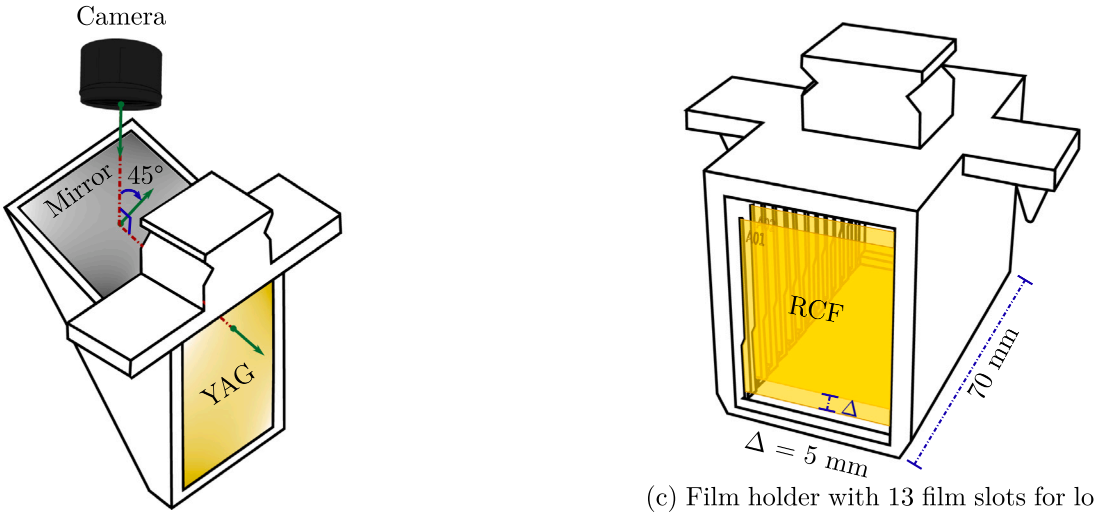

(b) The beam profile monitor.

(c) Film holder with 13 film slots for longitudinal dosimetry.

Fig. 3. Drawings of the robotic sample handling system and the 3D printed sample holders.

3. Experimental procedure

3.1. Irradiation

Radiochromic films were irradiated at multiple distances from the vacuum window, at both CONV and FLASH dose-rates. Each set of film irradiations was accompanied by longitudinal scans of the beam profile using a YAG screen. The aim is to assess the consistency of screen- and charge measurements with the dose readings from the RCFs—because this is an essential step in establishing the active dose-monitoring procedure.

3.2. RCF processing

The RCFs were calibrated against an Advanced Markus Chamber at conventional dose rate, using the 6 MeV Oriatron eRT6 electron linac at the Lausanne University Hospital [16]. To obtain the dose distributions, the RCFs were digitized at 300 dpi using a flatbed photo scanner, and pre-processed according to the procedures described in Ref. [17]. Moreover, the red channel was selected for dose evaluation, because this channel had the most sensitive calibration curves for the doses used.

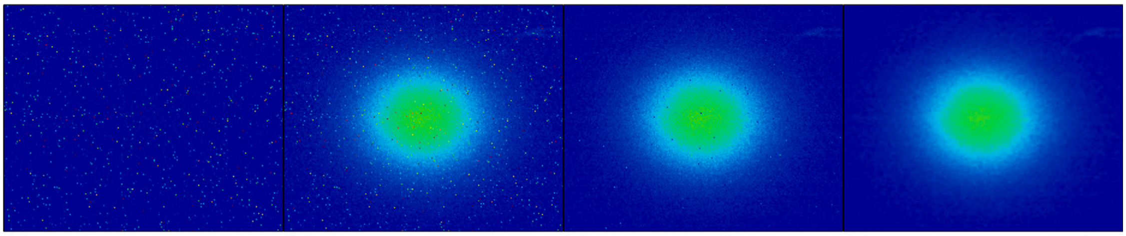

(a) Background signal without beam. (b) Unprocessed signal with beam. (c) Net signal after background subtraction. (d) Processed signal after median filtering.

Fig. 4. The effect of processing the digital images of YAG2.

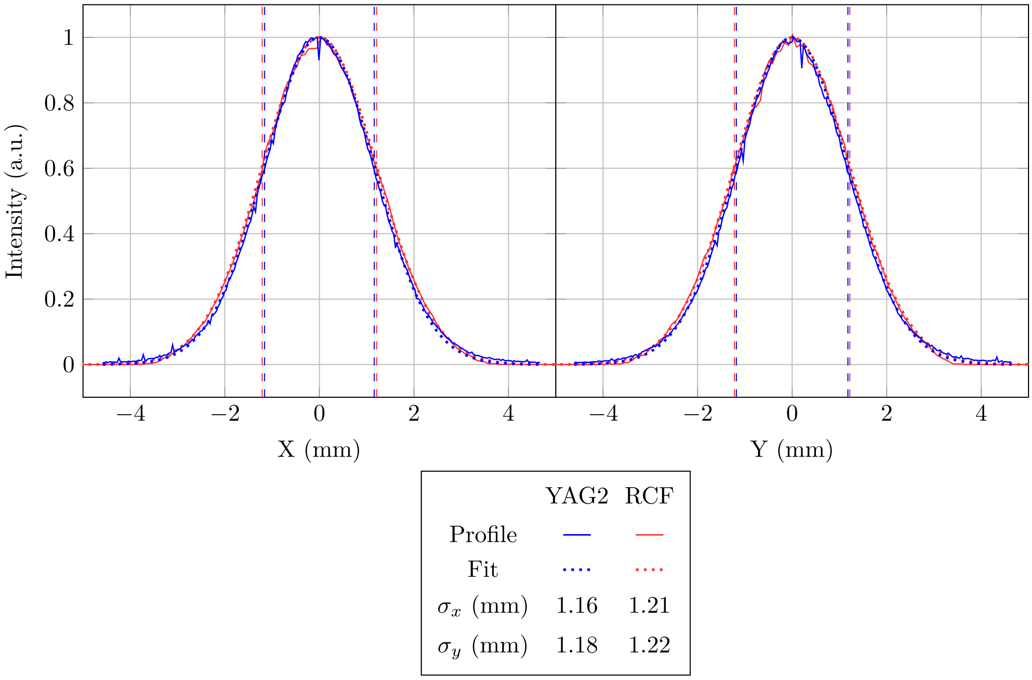

Fig. 5. The horizontal (left) and vertical (right) beam profiles obtained from an RCF and superimposed images from YAG2. The vertical lines indicate the transverse beam sizes σ_x and σ_y.

3.3. Image processing

Dosimetry with non-uniform beams, such as the Gaussian beam at CLEAR, requires particular care in measuring the distribution and beam alignment. An important step is therefore to define a metric for comparison of the transverse distributions of the RCF and the profile monitor. This metric must be independent of the absolute intensity of the profile monitor, so that a relationship between charge and dose distribution can be established.

Assuming a beam with no coupling between the horizontal and vertical planes, the beam charge density distribution acquired from the beam profile monitor can be described by the two-dimensional Gaussian distribution in Eq. (1),

$$Q'(x,y) = Q'_{\max} \cdot \exp\left[-\left(\frac{(x-\mu_x)^2}{2\sigma_x^2} + \frac{(y-\mu_y)^2}{2\sigma_y^2}\right)\right], \quad (1)$$

where $Q'_{\max} = Q'(\mu_x, \mu_y)$ is the charge density at the centre of the beam, σ_x and σ_y are the transverse beam sizes, and μ_x and μ_y are the coordinates of the mean. The mean coordinates (μ_x, μ_y) also define the reference point for the beam position. To be able to compare such parameters between different images in a systematic manner, it is imperative to remove any noise which is not related to the beam from the image. Fig. 4 shows the effect of background subtraction and subsequent application of a median filter. The first step of subtracting Figs. 4(a) from 4(b) ensures that any background signal is brought to zero. By applying a median filter to the resulting image in Fig. 4(c), the defective pixels are taken out.

It is worth noting that in CONV mode, several subsequent beam pulses will be accumulated in the same RCF. Since the YAG image acquisition is triggered with each pulse, these images should therefore be overlapped to take the beam position jitter into account. This superimposition ensures comparable distributions between the YAG image and the RCF. In FLASH mode, relative position jitter between the YAG and the RCF is not a concern, because the entire beam is delivered in a single pulse. Taking these considerations into account, the following procedure for image processing has been developed in python:

1. Starting with all images as two-dimensional arrays, the background is subtracted.
2. A 3 × 3 median filter is then applied.
3. For CONV, YAG images corresponding to the number of pulses are superimposed.
4. The beam centre $(\mu_x,\ \mu_y)$ is estimated by the maximum of the image projections in each direction.

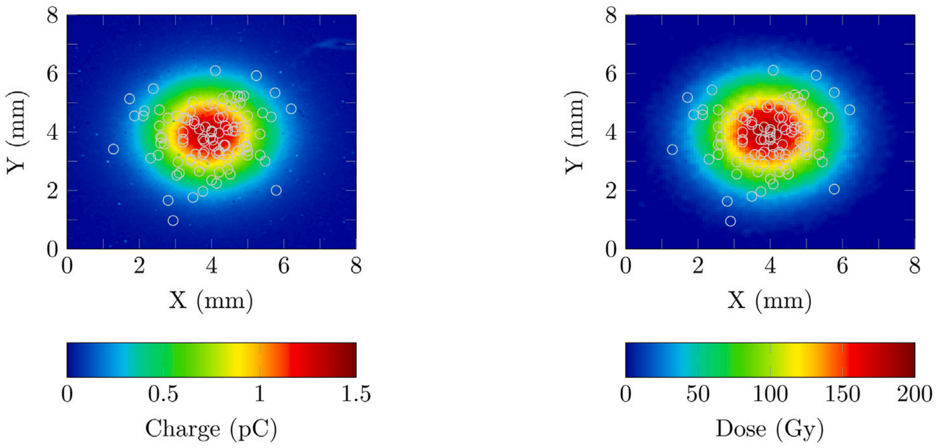

(a) Charge distribution.

(b) Dose distribution.

Fig. 6. The two dimensional distributions of (a) charge from YAG2 and ICT measurement and (b) dose from the film, with the local regions A_i indicated.

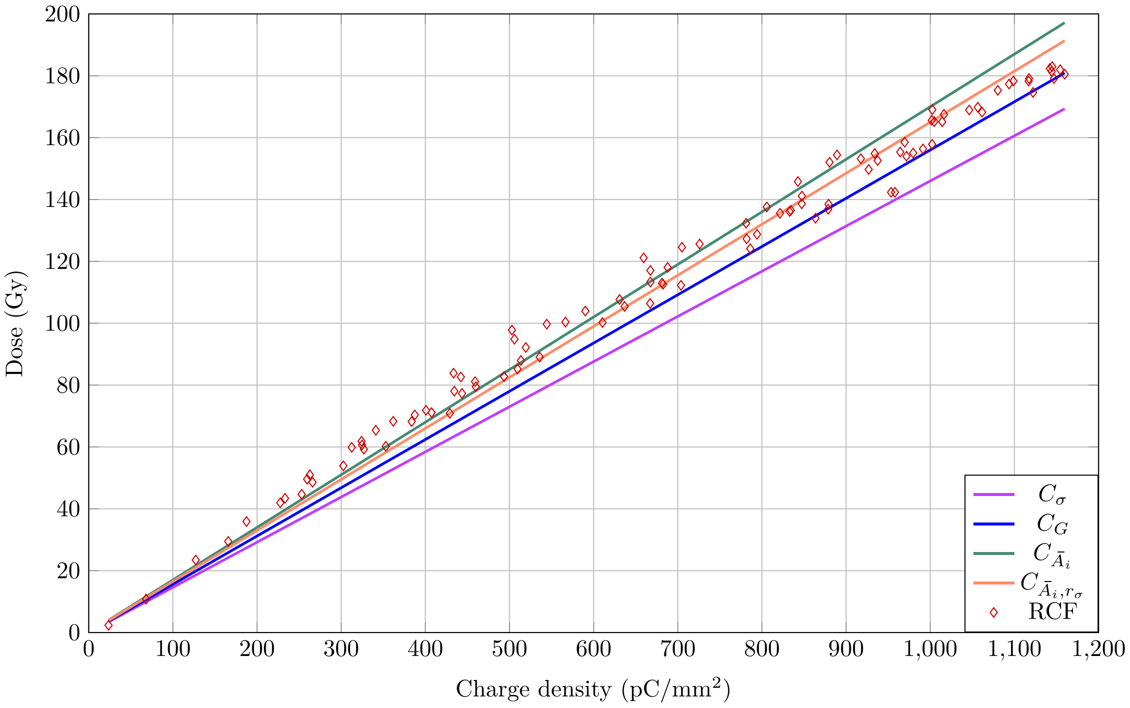

Fig. 7. Predicted doses using the calibration factors C_G, $C_{\bar{A}_i}$, $C_{\bar{A}_i,r_\sigma}$ and C_σ on the circles A_i in Fig. 6(a). The corresponding measured doses from Fig. 6(b) are shown in red.

5. Approximate values for σ_x and σ_y are estimated, and the images are cropped to $(\mu_x, \mu_y) \pm 5 \times (\sigma_x, \sigma_y)$.
6. Thin strips a few pixels wide around the centre are defined in x and y directions to generate the separate beam profiles.
7. A Gaussian fit is performed on the profiles to obtain the true values for μ_y, μ_y, σ_x, and σ_y.

After applying these steps, we will compare two different metrics of correlation between YAG and RCF distributions; namely the 1σ -beam size, and the overall intensity distribution.

3.4. Semi-analytical approach

Fig. 5 shows the horizontal and vertical profiles obtained via the procedure described in Section 3.3, for YAG2 and an HD-V2 RCF irradiated simultaneously in air under CONV conditions.

The deduced beam sizes indicate that the distributions from YAG2 and the RCF are in good agreement. The discrepancies between the two detectors are 4.3% and 3.4% for the horizontal and vertical planes, respectively.

The ICT measurement corresponds to the integral of the two-dimensional Gaussian function in Eq. (1), given by

$$Q_{\mathrm{tot}} = \int_{-\infty}^{\infty} \int_{-\infty}^{\infty} Q'(x, y)\ \mathrm{d}x\mathrm{d}y = 2\pi\sigma_x\sigma_y Q'_{\mathrm{max}}, \tag{2}$$

where Q_{tot} is the total charge and $Q'(x, y)$ is the local charge density. We assume that the dose distribution $D(x, y)$ is proportional to the charge density $Q'(x, y)$ in Eq. (1).

We may then estimate a calibration factor C_σ as the ratio between the D_{max} and Q'_{max}. Using the total accumulated charge of $Q_{\mathrm{tot}} = 10.65$ nC measured by the ICT combined with σ_x and σ_y from YAG2, we find $Q'_{\mathrm{max}} = 1238$ pC/mm^2. From the RCF we find a peak dose of

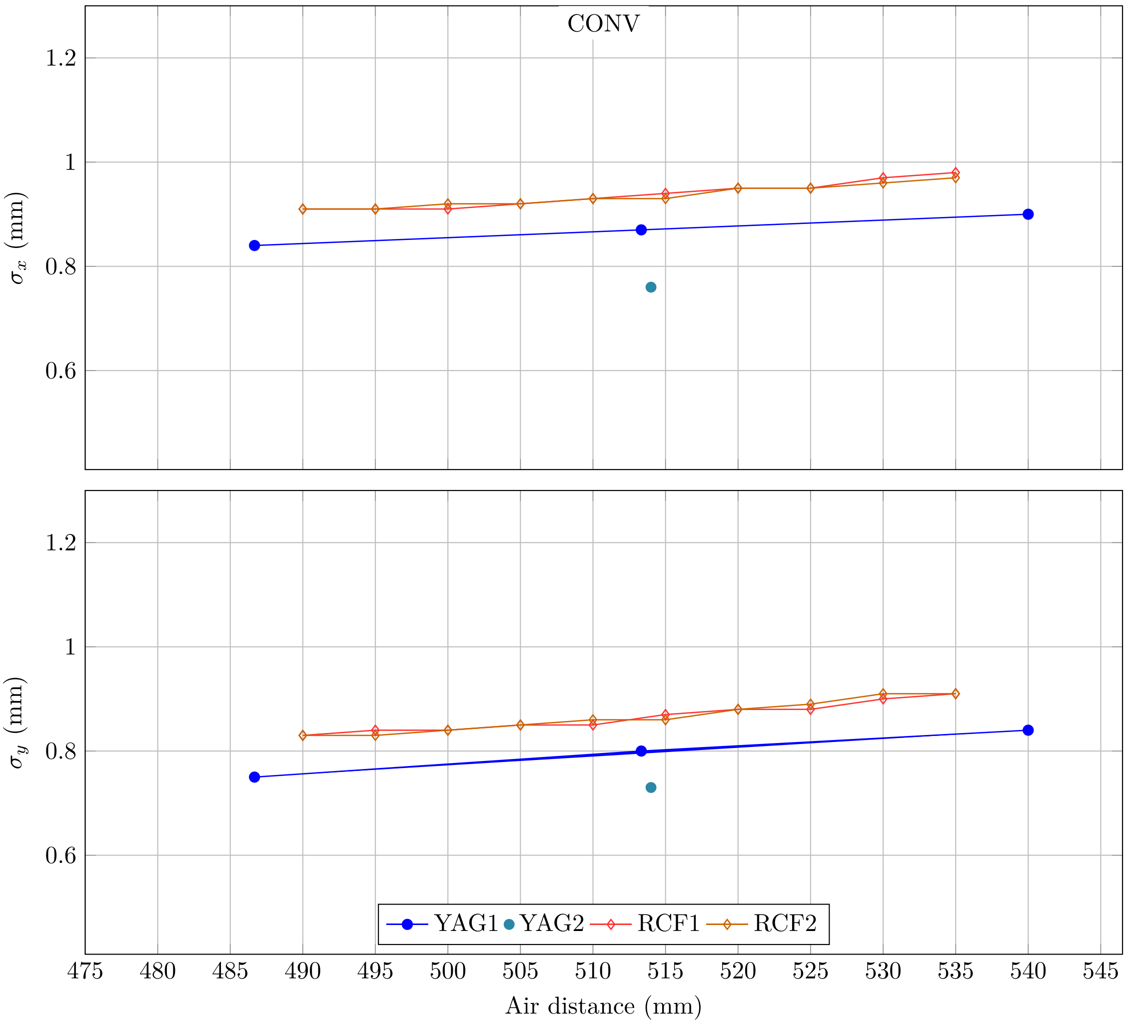

Fig. 8. The longitudinal evolution of the transverse beam sizes in horizontal (top) and vertical (bottom) directions, under CONV conditions.

$D_{\max} = D(\mu_x, \mu_y) = 181$ Gy, and we obtain

$$C_\sigma = \frac{D_{\max}}{Q'_{\max}} = 0.146 \ \frac{\text{Gy mm}^2}{\text{pC}}. \tag{3}$$

With this calibration factor, the expected transverse dose distribution for a given beam charge Q_{tot} and transverse beam sizes σ_x and σ_y can be estimated in air

$$D(x, y) = D_{\max} \cdot \exp\left[-\left(\frac{(x-\mu_x)^2}{2\sigma_x^2} + \frac{(y-\mu_y)^2}{2\sigma_y^2}\right)\right], \tag{4}$$

with

$$D_{\max} = \frac{C_\sigma}{2\pi} \cdot \frac{Q_{\text{tot}}}{\sigma_x \sigma_y}. \tag{5}$$

3.5. Numerical approach

We can also omit the assumption of a Gaussian distribution by looking directly at the charge density, and following the same procedure as described in Section 3.3. This method avoids any requirement regarding nature of the distribution, but is potentially more sensitive to un-physical artefacts of the monitoring system, such as noise and defective camera pixels. An accurate estimate of the beam position is important, and particularly in air, where the beam size is small relative to the pixel size.

The charge distribution Q_{xy} can be obtained from the YAG via Eq. (6), by normalization of the intensity distribution i_{xy} of the image, and scaling by the total delivered charge Q_{tot}.

$$Q_{xy} = Q_{\text{tot}} \cdot \frac{i_{xy}}{\sum_{xy} i_{xy}} \tag{6}$$

Fig. 6(a) shows the resulting charge distribution. The dose distribution D_{xy} in Fig. 6(b) is obtained from the RCF. One way to numerically estimate the calibration factor from charge density to dose is via the global integrals of the YAG and RCF distributions in Eq. (7)

$$C_G = \frac{P_R^2 \cdot \sum_{xy} D_{xy}}{\sum_{xy} Q_{xy}} = 0.156 \ \frac{\text{Gy mm}^2}{\text{pC}}, \tag{7}$$

where P_R is the pixel size of the RCF.

Another way is by sampling $N = 100$ normally distributed small circles A_i across the distributions. The size of the circles were chosen such that they are small enough to limit the local variation, yet large enough to contain the largest pixel size ($r \simeq 0.20$ mm $\ll \sigma$). The local ratio of dose to charge density is then determined by evaluating the mean dose across A_i from the dose distribution in Fig. 6(b), and the charge density of the corresponding area in the charge distribution in Fig. 6(a). The local calibration factor $C_{\bar{A}_i}$ can then be evaluated as the average of all local charge to dose density ratios;

$$C_{\bar{A}_i} = \frac{1}{N} \sum_i \frac{\overline{D(A_i)}}{\overline{Q'(A_i)}} = 0.170 \ \frac{\text{Gy mm}^2}{\text{pC}}. \tag{8}$$

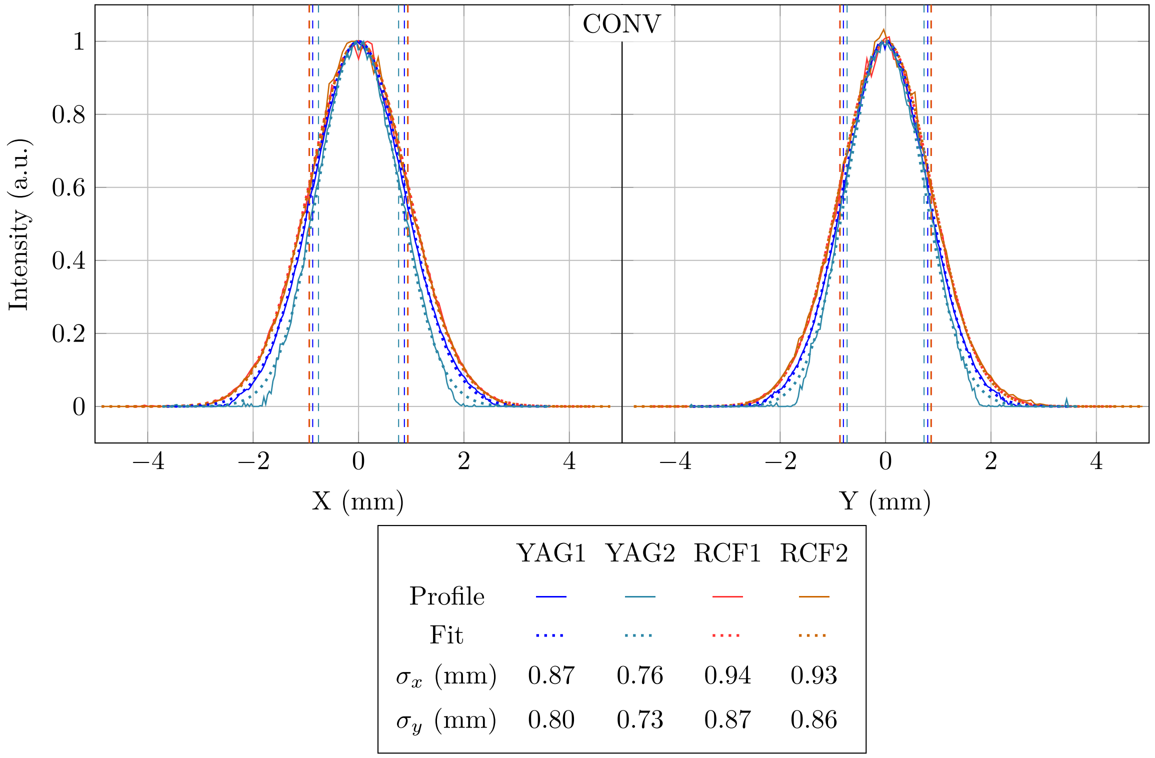

	YAG1	YAG2	RCF1	RCF2
Profile	—	—	—	—
Fit	····	····	····	····
σ_x (mm)	0.87	0.76	0.94	0.93
σ_y (mm)	0.80	0.73	0.87	0.86

Fig. 9. The horizontal (left) and vertical (right) beam profiles obtained from the films and YAG screens under CONV conditions. The vertical lines indicate the horizontal and vertical beam sizes σ_x and σ_y.

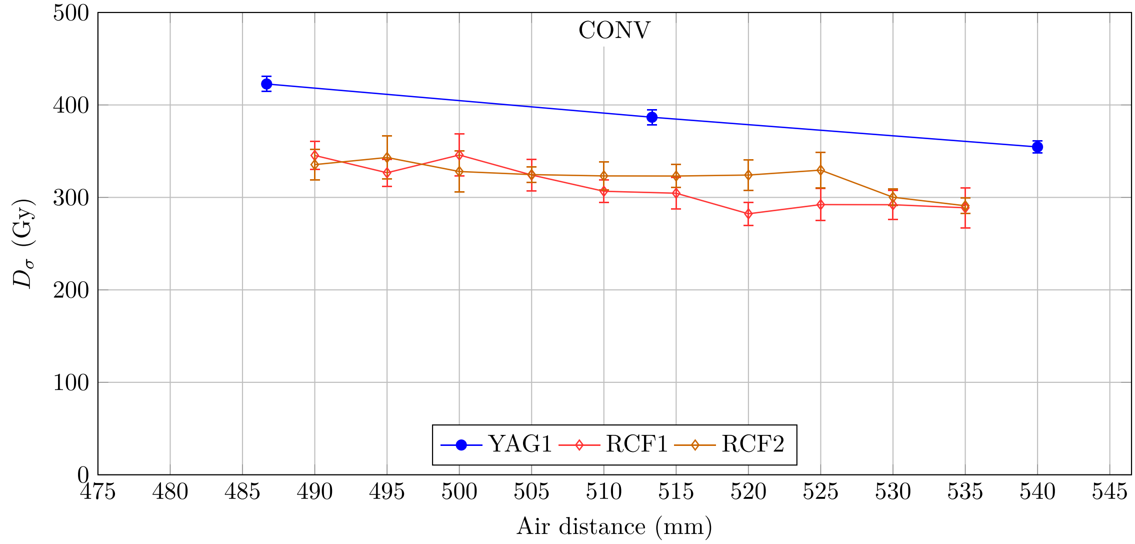

Fig. 10. The longitudinal evolution of the predicted and measured peak doses under CONV conditions.

A third option is to limit the calculation to the samples A_i that are located within e.g. $1-\sigma$ from the centre,

$$C_{\bar{A}_i,r_\sigma} = \frac{1}{N_{r<\sigma}} \sum_{i_{r<\sigma}} \frac{\overline{D(A_i)}}{\overline{Q'(A_i)}} = 0.165\ \frac{\mathrm{Gy\ mm^2}}{\mathrm{pC}}. \tag{9}$$

$C_{\bar{A}_i,r_\sigma}$ limits the contribution of the tails, a region in which the doses approach the lower limit of the dynamic range of the RCF, and the uncertainty increases. This calibration factor should therefore yield a better dose estimate for samples located within a radius of $1-\sigma$ of the beam centre.

3.6. *Method evaluation*

To evaluate the accuracy of the different calibration factors, we may then apply them to the charge density of each individual circle A_i in Fig. 6(a). Fig. 7 shows the measured dose of the circles in Fig. 6(b), as function of measured charge density of the corresponding circles in Fig. 6(a). The straight lines show the corresponding predicted doses using the calibration factors C_σ, C_G, $C_{\bar{A}_i}$ and $C_{\bar{A}_i,r_\sigma}$.

A comparison of the different calibration factors along with their average predictability overall and within a radius of 1σ can be seen in Table 4. If we omit points outside of the dynamic range of the RCF

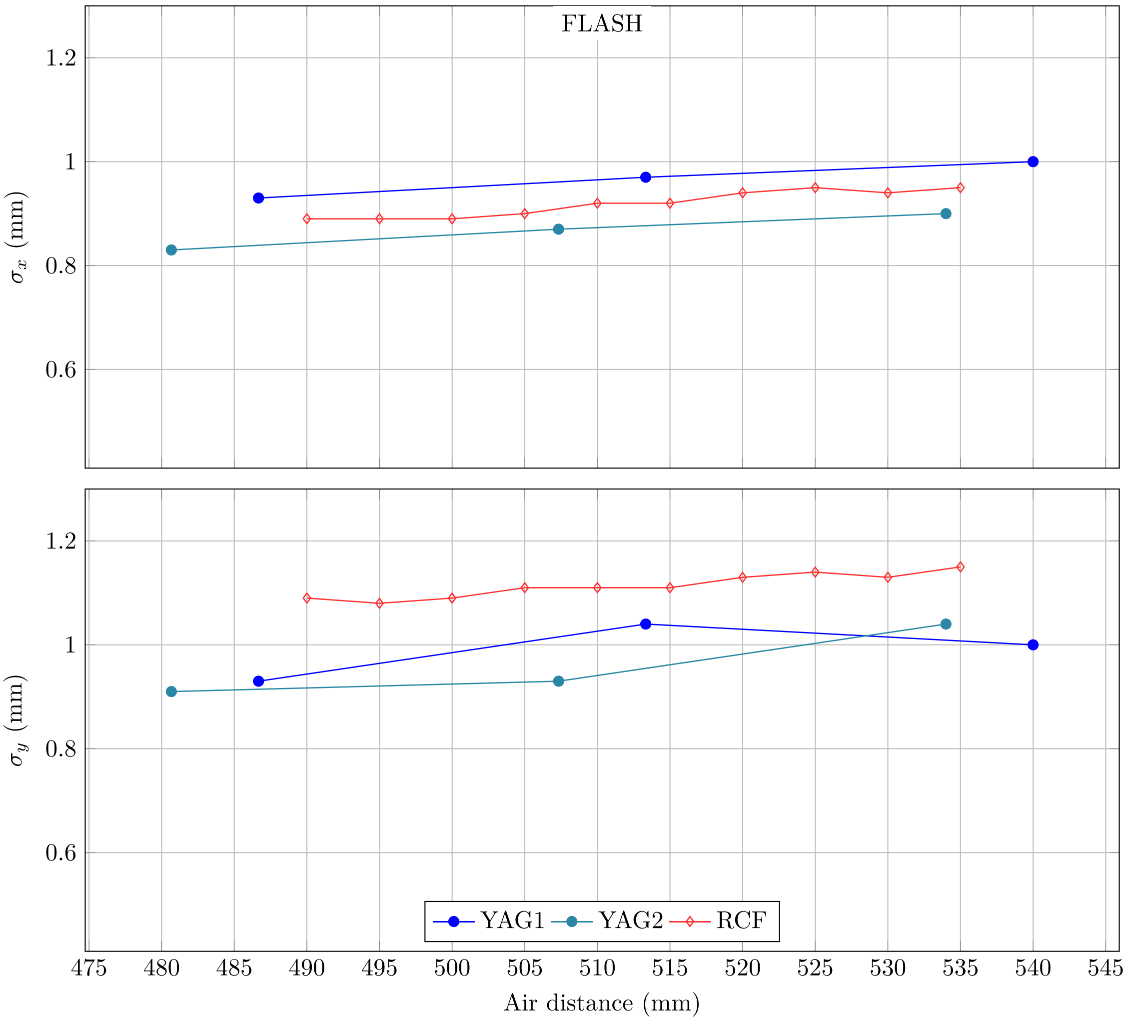

Fig. 11. The longitudinal evolution of the transverse beam sizes in horizontal (top) and vertical (bottom) directions, under FLASH conditions.

Table 4
Calibration factors obtained via the charge density method.

Calibration factors			
Factor	Value (Gy mm^2/pC)	Overall RMSPE	1σ RMSPE
C_σ	0.146	14.8%	11.1%
C_G	0.156	9.8%	5.8%
$C_{\bar{A}_i}$	0.170	6.5%	5.9%
$C_{\bar{A}_i,r_\sigma}$	0.165	6.8%	4.2%

(<10 Gy), the three numerical calibration factors C_G, $C_{\bar{A}_i}$ and $C_{\bar{A}_i,r_\sigma}$ all have RMS prediction errors of less than 10% overall. This error is reduced to 6% if we limit the prediction to within 1σ. The semi-analytical factor C_σ exhibits a predictability which is clearly below the numerical methods. $C_{\bar{A}_i,r_\sigma}$ seems to be best performing, with an average error of less than 5% for predictions within 1σ.

It is clear that all the calibration methods exhibit improved predictability close to the centre of the Gaussian distribution. This may be partly explained by the fact that the doses in this region are significantly offset from the edge of the dynamic range of the RCF.

4. Results and discussion

Using the system illustrated in Fig. 3, longitudinal scans in air were performed to study the longitudinal evolution of the beam profiles and dose, using both the YAG screen and two RCFs per position (RCF1 and RCF2). The performance of the calibration methods described in Section 3 was assessed via a separate set of measurements. As opposed to during the calibration, the profile monitors and RCFs were irradiated separately.

4.1. CONV mode

The measured beam sizes and their longitudinal evolution for the YAG screens and RCFs can be seen in Fig. 8. The graphs show the increase of the beam size as the beam expands in air. Both the RCFs and YAG1 measures a similar slope for the beam expansion. This indicates that the measurements from the RCFs and the YAG1 are in good agreement, apart from a systematic offset of about 10%. Whether or not this is a physical or instrumental issue is not fully understood. Only a single point for YAG2 was recorded due to data loss during the acquisition. Additionally, the transverse profiles for a single position (∼515 mm) are shown in Fig. 9.

The likely explanation for the difference between the profiles and beam sizes from YAG1 and YAG2 is that the gain setting was too low for the amount of light emitted by YAG2 in CONV mode. The same gain was used for both screens, and with YAG1 being thicker than YAG2, it is expected that it will emit more light. By looking at the profiles it appears that the signal-to-noise ratio (S/N) is too low in the tails of the YAG2 profile in Fig. 9. Moreover, the ∼10% discrepancy between YAG1 and the RCFs is also slightly higher than what was found during the calibration in Fig. 5. The gain could also play a role in explaining

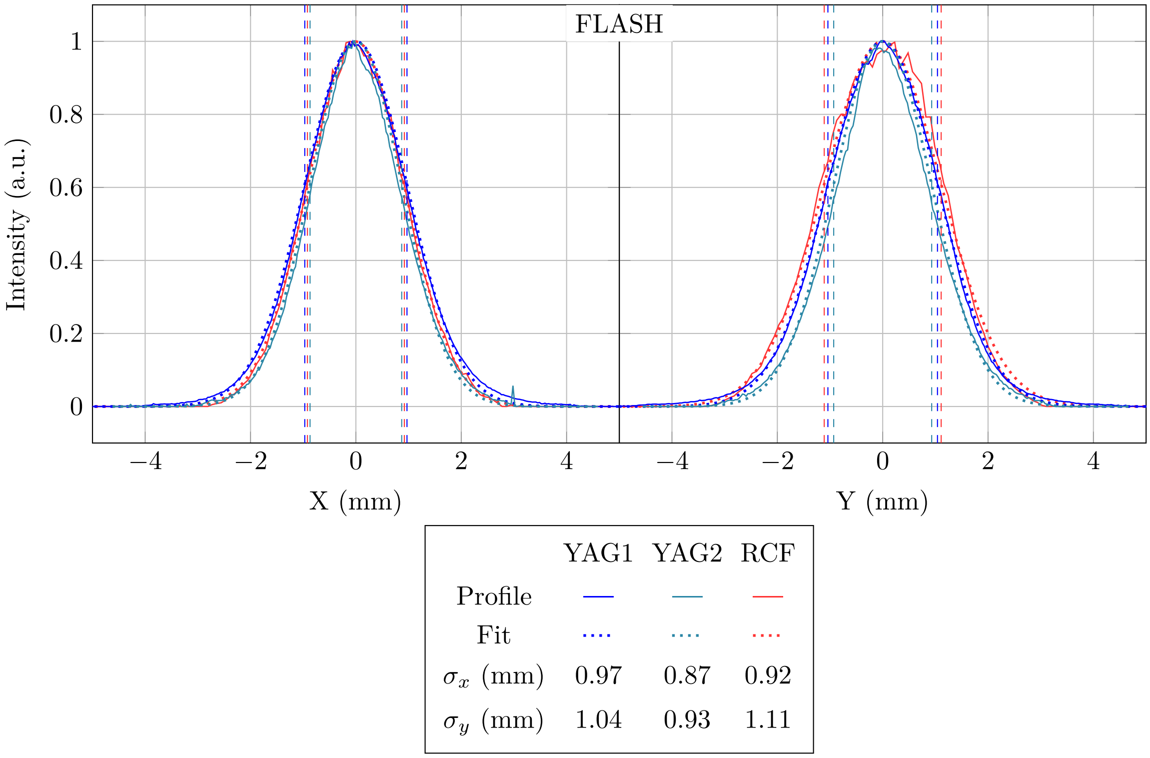

	YAG1	YAG2	RCF
Profile	—	—	—
Fit	····	····	····
σ_x (mm)	0.97	0.87	0.92
σ_y (mm)	1.04	0.93	1.11

Fig. 12. The horizontal (left) and vertical (right) beam profiles obtained from the films and YAG screens under FLASH conditions. The vertical lines indicate the horizontal and vertical beam sizes σ_x and σ_y.

this, but the difference in timing for the YAG and RCF irradiation could also have an impact. The YAG and RCF were irradiated simultaneously during the calibration, while approximately two hours apart during the experiment. One potential explanation for the discrepancy between the two irradiations could therefore be variations in beam stability.

If we then look at how well the calibration factor $C_{\bar{A}_i, r_\sigma}$ in Table 4 describes the dose evolution, we see from Fig. 10 that the slopes are again similar. However, there is an offset of about 15% between the predicted peak dose from YAG1 and the corresponding dose measured on the RCF. The main explanation for this is directly linked to the beam size discrepancy in Fig. 8; if the apparent beam size is lower, then the predicted peak dose will be higher. Another potential contributing error here, is the fact that for the beam size in question, the pixel size of the digitized RCF is relatively large, and the peak region is thus composed of a single pixel.

4.2. FLASH mode

The same experiment as in Section 4.1 was then done in FLASH mode for comparison. Apart from the beam mode, the only differences were that only a single longitudinal film holder was used, and the full data set was collected within approximately 30 min. The resulting beam size evolution from the longitudinal scans can be seen in Fig. 11, and the transverse profiles for a single position (∼515 mm) are shown in Fig. 12.

In the horizontal direction, we see clearly that the slopes of the beam size evolution of YAG1, YAG2 and the RCF are similar. The discrepancies between YAG2 and the RCFs are now at about 5%, which is very likely to be due to the increased S/N that comes with the higher charge per pulse in FLASH mode. As for YAG1, we see that in FLASH mode, there is an overestimation of the beam size of about 5% relative to that of the RCF. In light of the underestimation observed for the CONV mode in Section 4.1, this may indicate that the S/N was too low for YAG1 in CONV mode. If we look at the vertical direction, the results are a bit more difficult to interpret, but there is still a clear correlation between the YAG screens and the RCFs.

Looking at the measurements and predictions of the peak dose evolution in Fig. 13, we see a reasonably good agreement, particularly between YAG1 and the RCF with less than 10% discrepancy. Additionally, the uncertainty related to the small beam size relative to the pixel size of the digitized RCF remains.

5. Summary and conclusions

It has been demonstrated that the combination of a YAG:Ce scintillating screen and an ICT can be used for dose prediction with a predictability of up to 95%. It has also been shown that using both beam size or charge density from beam profile monitors to predict the dose deposition is feasible. It was found that the accuracy of the presented method is particularly sensitive to the camera settings relative to the amount of light emitted. In order to achieve reproducible and reliable dosimetry, it remains to perform a full correlation study between the camera setting, screen thickness and charge density, to ensure that the system is producing a signal within the linear range of the camera. Another limiting factor of the presented data is the relatively large pixel size of the digitized RCFs relative to the beam size. Achieving good control of the combination of camera- and beam parameters should allow for stable dose predictions with less than 5% error for a Gaussian beam.

5.1. Future work

Research activities are already on-going for testing and characterization of a system for generating a flat profile in the transverse plane for VHEE beams at CLEAR. With a flat profile, the issues of S/N in the tails of the distribution and pixel size limitations are expected to be of much less importance.

Finally, it remains to calibrate these measurements to dose in water. With the link between beam profile and charge in air to dose in water,

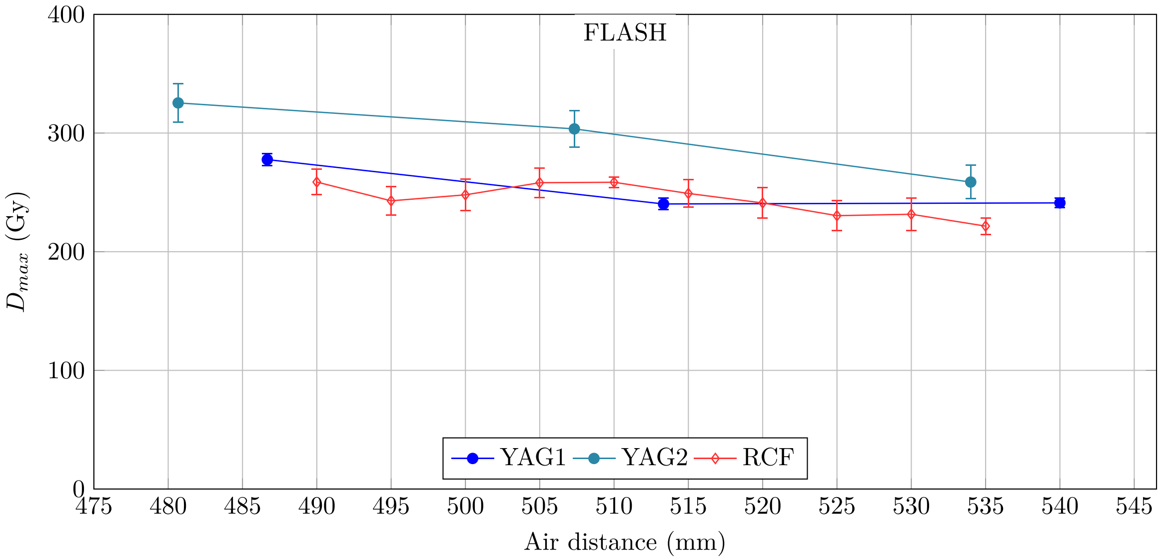

Fig. 13. The longitudinal evolution of the predicted and measured peak doses in FLASH conditions.

it should be possible to predict the delivered dose for both CONV and FLASH conditions, while simultaneously retrieve the information about the transverse dose distribution. Such a dosimetry system would be very useful for clinical studies of FLASH radiotherapy and VHEE.

CRediT authorship contribution statement

Vilde F. Rieker: Writing – review & editing, Writing – original draft, Visualization, Validation, Software, Methodology, Investigation, Formal analysis, Data curation. **Roberto Corsini:** Writing – review & editing, Writing – original draft, Supervision, Resources, Project administration, Investigation, Conceptualization. **Steinar Stapnes:** Writing – review & editing, Writing – original draft, Supervision, Project administration. **Erik Adli:** Writing – review & editing, Writing – original draft, Supervision, Funding acquisition. **Wilfrid Farabolini:** Software, Methodology, Investigation. **Veljko Grilj:** Investigation. **Kyrre N. Sjobak:** Supervision, Software. **Laurence M. Wroe:** Writing – review & editing, Formal analysis, Conceptualization. **Avni Aksoy:** Software, Investigation. **Cameron S. Robertson:** Software. **Joseph J. Bateman:** Software. **Pierre Korysko:** Writing – review & editing, Investigation. **Alexander Malyzhenkov:** Writing – review & editing, Investigation. **Antonio Gilardi:** Investigation. **Manjit Dosanjh:** Writing – review & editing, Supervision.

Declaration of competing interest

The authors declare that they have no known competing financial interests or personal relationships that could have appeared to influence the work reported in this paper.

Data availability

Data will be made available on request.

Acknowledgements

This work was supported by the Research Council of Norway (NFR grant no. 310713).

References

[1] M.-C. Vozenin, P. De Fornel, K. Petersson, V. Favaudon, M. Jaccard, J.-F. Germond, B. Petit, M. Burki, G. Ele Ferrand, D. Patin, H. Bouchaab, M. Ozsahin, F. Bochud, C. Bailat, P. Devauchelle, J. Bourhis, The advantage of FLASH radiotherapy confirmed in mini-pig and cat-cancer patients, Clin. Cancer Res. : Off. J. Am. Assoc. Cancer Res. 25 (1) (2019) 35–42, http://dx.doi.org/10.1158/1078-0432.CCR-17-3375, URL http://clincancerres.aacrjournals.org/.

[2] M. McManus, F. Romano, N.D. Lee, W. Farabolini, A. Gilardi, G. Royle, H. Palmans, A. Subiel, The challenge of ionisation chamber dosimetry in ultra-short pulsed high dose-rate Very High Energy Electron beams, Sci. Rep. 10 (1) (2020) 9089, http://dx.doi.org/10.1038/s41598-020-65819-y, URL https://www.nature.com/articles/s41598-020-65819-y.

[3] F. Di Martino, P. Barca, S. Barone, E. Bortoli, R. Borgheresi, S. De Stefano, M. Di Francesco, L. Grasso, G. Lucia, S. Linsalata, D. Marfisi, M. Pacitti, G. Felici, L. Faillace, FLASH radiotherapy with electrons: Issues related to the production, monitoring, and dosimetric characterization of the beam, Front. Phys. 8 (2020) http://dx.doi.org/10.3389/fphy.2020.570697.

[4] M. Sharma, R. Singh, N. Robert, G. Trivedi, P. Tomar, A.S. Oinam, Beam quality and dose rate dependency of Gafchromic EBT3 film irradiated with therapeutic megavolt photon beams, Radiat. Meas. 146 (2021) 106632, http://dx.doi.org/10.1016/J.RADMEAS.2021.106632.

[5] E.Y. León-Marroquín, D.J. Mulrow, R. Khan, A. Darafsheh, Spectral analysis of the EBT3 radiochromic films for clinical photon and electron beams, Med. Phys. 46 (2) (2019) 973–982, http://dx.doi.org/10.1002/MP.13330.

[6] M. Jaccard, K. Petersson, T. Buchillier, J.F. Germond, M.T. Durán, M.C. Vozenin, J. Bourhis, F.O. Bochud, C. Bailat, High dose-per-pulse electron beam dosimetry: Usability and dose-rate independence of EBT3 Gafchromic films, Med. Phys. 44 (2) (2017) 725–735, http://dx.doi.org/10.1002/MP.12066.

[7] L. Karsch, E. Beyreuther, T. Burris-Mog, S. Kraft, C. Richter, K. Zeil, J. Pawelke, Dose rate dependence for different dosimeters and detectors: TLD, OSL, EBT films, and diamond detectors, Med. Phys. 39 (5) (2012) 2447–2455, http://dx.doi.org/10.1118/1.3700400.

[8] A. Lagzda, D. Angal-Kalinin, J. Jones, A. Aitkenhead, K.J. Kirkby, R. MacKay, M. Van Herk, W. Farabolini, S. Zeeshan, R.M. Jones, Influence of heterogeneous media on Very High Energy Electron (VHEE) dose penetration and a Monte Carlo-based comparison with existing radiotherapy modalities, Nucl. Instrum. Methods Phys. Res. B 482 (2020) 70–81, http://dx.doi.org/10.1016/J.NIMB.2020.09.008.

[9] K.N. Sjobak, E. Adli, C.A. Lindstrom, M. Bergamaschi, S. Burger, R. Corsini, A. Curcio, S. Curt, S. Doebert, W. Farabolini, D. Gamba, L. Garolfi, A. Gilardi, I. Gorgisyan, E. Granados, H. Guerin, R. Kieffer, M. Krupa, T. Lefevre, S. Mazzoni, G. McMonagle, H. Panuganti, S. Pitman, V. Rude, A. Schlogelhofer, P.K. Skowronski, M. Wendt, A. Zemanek, S.J. Nadenau, F. Jülich, G.A. Lyapin, J. at Royal Holloway, Status of the clear electron beam user facility at cern, in: Proceedings of the 10th International Particle Accelerator Conference, Melbourne, Australia, 2019, pp. 983–986, http://dx.doi.org/10.18429/JACoW-IPAC2019-MOPTS054.

[10] D. Gamba, R. Corsini, S. Curt, S. Doebert, W. Farabolini, G. Mcmonagle, P.K. Skowronski, F. Tecker, S. Zeeshan, E. Adli, C.A. Lindstrøm, A. Ross, L.M. Wroe, The CLEAR user facility at CERN, Nucl. Inst. Methods Phys. Res. 909 (2018) 480–483, http://dx.doi.org/10.1016/j.nima.2017.11.080.

[11] P. Korysko, M. Dosanjh, J. Bateman, C. Robertson, R. Corsini, W. Farabolini, A. Aksoy, A. Malyzhenkov, V. Rieker, S.K. N Sjobak, The CLEAR user facility: A review of the experimental methods and future plans, in: Proceedings of the 14th International Particle Accelerator Conference, 2023, pp. 876–879, http://dx.doi.org/10.18429/JACoW-IPAC2023-MOPL141, URL https://accelconf.web.cern.ch/ipac2023/.

[12] A. Basler, Aca1920-40gm | basler product documentation, 2024, URL https://docs.baslerweb.com/aca1920-40gm.

[13] Crytur, YAG:Ce | Crytur.cz, 2023, URL https://www.crytur.cz/materials/yagce/.

[14] B. Instrumentation, Bergoz – FCT - Very fast non-destructive pulsed or CW beams observation, 2023, URL https://www.bergoz.com/products/fct/.

[15] Ashland, Gafchromic™ HD-V2 films, 2021, URL https://www.ashland.com/industries/medical/gafchromic-dosimetry-films/hdv2.

[16] M. Jaccard, M.T. Durán, K. Petersson, J.F. Germond, P. Liger, M.C. Vozenin, J. Bourhis, F. Bochud, C. Bailat, High dose-per-pulse electron beam dosimetry: Commissioning of the Oriatron eRT6 prototype linear accelerator for preclinical use, Med. Phys. 45 (2) (2018) 863–874, http://dx.doi.org/10.1002/MP.12713.

[17] V. Rieker, J.J. Bateman, W. Farabolini, P. Korysko, Development of reliable VHEE/FLASH passive dosimetry methods and procedures at CLEAR, in: Proceedings of the 14th International Particle Accelerator Conference, Venice, Italy, 2023, pp. 5028–5031, http://dx.doi.org/10.18429/JACoW-IPAC2023-THPM060, URL https://accelconf.web.cern.ch/ipac2023/.